Creating innovative composite materials to enhance the kinetics of CO 2 capture by hydroquinone clathrates

Romuald Coupan, Frédéric Plantier, Jean-Philippe Torré, Christophe Dicharry, Pascale Senechal, Fabrice Guerton, Peter Moonen, Abdel Khoukh, Sid Ahmed Kessas, Mehrdji Hemati

Creating innovative composite materials to enhance the kinetics of CO_2 capture by hydroquinone clathrates

Romuald Coupan [a], Frédéric Plantier [b], Jean-Philippe Torré [a,*], Christophe Dicharry [a], Pascale Sénéchal [c], Fabrice Guerton [c], Peter Moonen [a,c], Abdel Khoukh [d], Sid Ahmed Kessas [e], Mehrdji Hemati [e]

[a] CNRS/TOTAL/UNIV PAU & PAYS ADOUR, Laboratoire des Fluides complexes et leurs Réservoirs-IPRA, UMR5150, 64000 Pau, France
[b] CNRS/TOTAL/UNIV PAU & PAYS ADOUR, Laboratoire des Fluides complexes et leurs Réservoirs-IPRA, UMR5150, 64600 Anglet, France
[c] UNIV PAU & PAYS ADOUR, CNRS, DMEX-IPRA, UMS 3360, 64000 Pau, France
[d] UNIV PAU & PAYS ADOUR, CNRS – UMR 5254 – Institut des Sciences Analytiques et de Physico-Chimie pour l'Environnement et les Matériaux (IPREM), Hélioparc, Avenue du Président Pierre Angot, Pau F-64000, France
[e] Université de Toulouse – Paul Sabatier, CNRS – UMR 5503 – Laboratoire de Génie Chimique (LGC), ENSIACET, INPT, 5 rue Paulin Talabot, BP 1301, Toulouse F-31106, France

- Hydroquinone (HQ) clathrates were tested for CO_2 capture and storage applications.
- Composite materials were developed by impregnating porous silica particles with HQ.
- Materials were characterized and kinetics experiments with CO_2 were carried out.
- Results showed that reactive media are kinetically more efficient than powdered HQ.

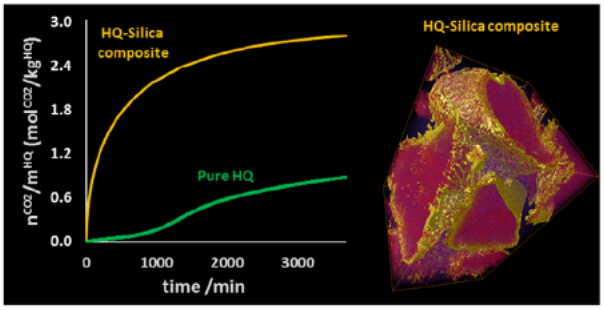

This study addresses both the preparation of a reactive medium composed of porous particles impregnated with hydroquinone (HQ), an organic compound capable of forming gas clathrates, and an evaluation of the kinetic performance of these composite materials for CO_2 capture. Two types of porous silica particles of different sizes and pore diameters were tested. The porous particles were impregnated with HQ by a dry impregnation (DI) method in a fluidized bed, and by a wet impregnation (WI) method. The impregnation effectiveness of the two methods is discussed, and the reactivity of the composite materials formed in terms of CO_2 capture and storage capacity is studied experimentally. The experimental results showed that the HQ adheres well on the silica without any chemical modification of the deposit's structure. We demonstrated that the impregnation technique plays a very important role in the kinetics of CO_2 capture. A series of experiments performed using a magnetic suspension balance at 3.0 MPa and 323 K showed that the silica based impregnated particles reversibly capture and store CO_2, and that the CO_2 capture kinetics are significantly enhanced compared to the results obtained with pure powdered HQ. Finally, we demonstrated that CO_2 capture is faster with dry impregnated particles.

Keywords:
Hydroquinone
Clathrates
Impregnation
Kinetics
CO_2 capture and storage

1. Introduction

Gas clathrates are inclusion compounds formed when "guest" molecules of gas are enclosed in "host" lattices [1]. Many species

* Corresponding author.
E-mail address: jean-philippe.torre@univ-pau.fr (J.-P. Torré).

http://dx.doi.org/10.1016/j.cej.2017.05.038
1385-8947

with a low molecular weight, such as carbon dioxide (CO_2), methane (CH_4) and nitrogen (N_2), can be trapped as guest molecules in a clathrate structure. A variety of host molecules, such as water, phenol and hydroquinone (HQ), have been studied in recent years and are described in literature [2]. Scientists have been fascinated by gas clathrates for more than a century, but these solid compounds are now the focus of even greater attention owing to their possible practical applications such as CO_2 capture and sequestration. This new interest arises from their capacity to store large quantities of gases, more or less selectively depending on the clathrates considered and the gas mixture used.

To begin with, the most studied clathrate compounds are "gas hydrates" [3], which generally form at high pressure (a few MPa) and low temperature (a few K above 273 K) with water and gas. For the past 15 years or more, they have been the focus of many studies [4], which included adding chemical promoters or using different multiphase contactors [5–7] to overcome the many critical limitations that prevent hydrate based gas separation processes from being deployed, from pilot to industrial scale. However, the use of gas hydrates to separate CO_2 from gas mixtures such as CO_2/CH_4 and CO_2/N_2 is still hindered by the following main obstacles: (i) the overall cost of the process is not competitive compared to others such as reactive absorption [8], except when the raw gas is already pressurized (as the gas compression costs are prohibitive in most cases); (ii) the difficulties in handling, contacting and transporting a multiphase mixture composed of at least three phases that have to coexist (water or water/oil mixture, gases and solids) for the reaction to take place; (iii) the necessity to maintain a relatively low temperature in the apparatus for the gas hydrates to form (generally slightly above 273 K); and (iv) the low rate of hydrate formation and insufficient selectivity of gas hydrates toward CO_2 in certain gas mixtures, particularly CO_2/CH_4 [9,10].

Secondly, HQ is a solid hydroxy aromatic compound recently identified in literature as a potential innovative clathrate candidate for gas storage and separation [11–13]. Interestingly, for different gas mixtures such as CO_2/N_2, CO_2/H_2 and CO_2/CH_4 [14,15], the enclathration reaction with HQ seems to be highly selective to CO_2. The thermodynamic pressure temperature conditions (i.e. the clathrate phase equilibria) in which some HQ clathrates form and dissociate are mentioned in literature [16–19] and the equilibrium data and detailed characterization of CO_2 HQ clathrates were recently published [20–21]. But although HQ clathrates seem very interesting for practical applications such as CO_2 separation by direct gas/solid reaction (i.e. without using any solvent), the gas clathrate formation kinetics need to be improved before these compounds can be used on an industrial scale. Previous studies involving tests carried out using powdered HQ have already attempted to do so [14,15,22]. But very fine HQ particles would be difficult to handle in an industrial gas solid contactor (such as a fixed bed reactor) for several reasons: (i) the gas circulating through the HQ powder causes a significant pressure drop that in some cases could be excessive, (ii) the very fine particles can be blown into the process equipment, and (iii) operators must apply stringent safety measures when handling large quantities of a fine pulverulent material such as HQ during loading and unloading of the reactor. Indeed, reactivity is limited by the contact area between the gas and the solid HQ, and depends on the specific area of the reactive medium used. Consequently, in an attempt to enhance the gas–solid enclathration reaction, we developed a composite material made of porous particles impregnated with HQ that can be used as a reactive medium in a clathrate based gas separation process.

There are two procedures for impregnation: wet impregnation (abbreviated as WI below) and dry impregnation (abbreviated as DI below) in a fluidized bed. Creation of a composite material by WI consists of a dip coating method involving several steps: impregnation, filtration and drying [23]. DI in a fluidized bed was previously developed in the *Laboratoire de Génie Chimique* (chemical engineering laboratory) of Toulouse and patented by the INPT and the CNRS in 2001 [24]. Unlike WI, creation of a composite material by DI in a fluidized bed is a "one pot process" in which the stages of impregnation, filtration and drying are carried out in just one apparatus. This technique consists in spraying a solution containing the organic precursor onto a warm fluidized bed of porous particles chosen as the support material for the precursor. This condensed technique was initially used for depositing metal nanoparticles on porous supports (such as silica gel, alumina and activated carbon) and has shown that in operating conditions: (i) the deposition efficiency is close to 100%, (ii) the deposit is quasi uniform, and (iii) the size of the supported metal nanoparticles is controlled by the pore diameter [25–29]. In the present work, the composite materials synthesized by the two procedures (i.e. WI and DI) are evaluated as reactive media for CO_2 capture. Both the gas storage capacity of the reactive media and data on the CO_2 capture kinetics were measured and compared to the results obtained with pure powdered HQ. All experiments were performed at 3.0 MPa and 323 K by means of a gravimetric method using a magnetic suspension balance. These experimental conditions were chosen for two main reasons: (i) CO_2 HQ clathrates can form under relatively high temperature (e.g. 323 K) and pressure [20] conditions, which could be economically very advantageous when the raw gas is already hot and pressurized, the case for example of a production gas containing CO_2/CH_4; (ii) CO_2 HQ clathrates may reach their maximum capacity when the formation pressure is close to 3.0 MPa [30], justifying the operating pressure chosen for these tests.

2. Experimental section

2.1. Materials

The organic precursor used in this study is HQ (purity of 99.5 mol%) provided by Acros Organics. The solvent used in WI and DI is absolute ethanol (purity greater than 99 mol%). This choice was motivated by the high solubility of HQ in this solvent (e.g. 0.2063 mol% at 308.2 K) [31] and its low boiling temperature of 351 ± 2 K (calculated mean values obtained from the NIST) that facilitates the drying step. The N_2, CO_2 and helium (He) used for the experiments (minimum mole fraction purity of 99.995%) are purchased from Linde Gas SA. The porous supports used are silica particles provided by SiliCycle. The experiments are conducted with two types of silica particles: high grade irregular silica particles (SiliaFlash®, referred to as SF below) and high purity analytical grade spherical silica particles (SiliaSphere®, referred to as SS below) with tight particle size distribution. Information concerning native SF and SS particles is given in the Supplementary Material.

2.2. Experimental set up and methods

Prior to impregnation, a saturated solution of HQ in ethanol was prepared at 308 K based on the solubility data and a correlation proposed by Li and coworkers [31]. Before each experiment, the solid particles were dried for 24 h at 423 K in a muffle furnace (from Nabertherm).

2.2.1. Wet impregnation

WI is performed in hermetic glass vessels. An oven (model 800, from Memmert) is used to maintain the temperature at a constant value with an accuracy of ±0.5 K. A vacuum filtration system composed of a Buchner funnel connected to a vacuum pump is used for

the filtration step. Low porosity filters of 185 mm in diameter and with a pore size of 20 25 μm are placed at the bottom of the Buch ner funnel. This method consists in soaking the native support material in the HQ solution for 24 h at 308 K. During this step, the pores are first saturated with the HQ solution by capillarity. The impregnated particles are then filtered and placed in the oven to dry at 308 K for 24 h. Several previous studies have shown that the drying step is crucial when there is no strong interaction between the support material and the impregnation solution. Indeed, the species deposited in the pores of the support material during impregnation could be redistributed during the drying step, determining both the deposit location and its dispersion in the por ous matrix [32 34].

2.2.2. Dry impregnation

The DI experiments are carried out in a batch fluidized bed reac tor under an inert N_2 atmosphere. The equipment, shown in Fig. 1, built according to ATEX standards, makes it possible to treat 0.2 to 3.0 kg of particles in one go. The reactor is a Pyrex cylindrical col umn, 0.5 m high with an inner diameter of 0.1 m, topped by a 0.2 m conical freeboard set at 45°. The sidewall of the bed is transparent and allows observation of the various physical phenomena (e.g. the different fluidization regimes and the expansion of the particle bed) that occur inside the column during the impregnation pro cess. The fluidization gas enters the column through a distributor composed of a perforated stainless steel plate (porosity of 0.5%) under which is placed a metallic close meshed grid that prevents fine particles from passing through the distributor. Before the flu idization gas enters the bed, its flow rate is measured by rotame ters (Sho Rate model, from Serv'Instrumentation) which are calibrated to give a value with an accuracy of 3%. The fluidization gas is preheated by an electrical heater (4 kW). The elutriated par ticles are collected by two cyclones at the column outlet. The sol vent vapor is recovered by two home made condensers 1.0 m high with a shell inner diameter of 0.07 m. The first condenser is a water cooled coaxial heat exchanger and the second is a multi tubular heat exchanger (5 tubes) cooled by an aqueous solution of propylene glycol at 243 K chilled by a cryostat (Proline RP 1290 from Lauda). The precursor solution, stored in a vessel placed on a precision balance (PG5001 S from Mettler Toledo) to monitor the flow rate of the solution, is injected through an internal mixing two fluid spray nozzle (from Spray System Co.) using a volumetric pump (from LMI). The atomizing gas (N_2 or dried air) flow rate is controlled by a needle valve and measured by a rotameter similar to the one used for the fluidization gas. The atomizing nozzle is downward facing and located in the bed. The bed temperature is controlled by means of a PID regulator. Temperature and pressure drops are monitored during the operation by means of Pt100 probes (accuracy of ±0.2 K) and a 0 5 kPa Keller differential pres sure transducer (uncertainty of ±0.01 kPa) located across the bed.

The general experimental protocol is as follows. The column is initially loaded with a given mass of porous particles (about 300 g). The bed is fluidized with preheated air, to reach the set point temperature of 308 K. Indeed, a few studies concerning the

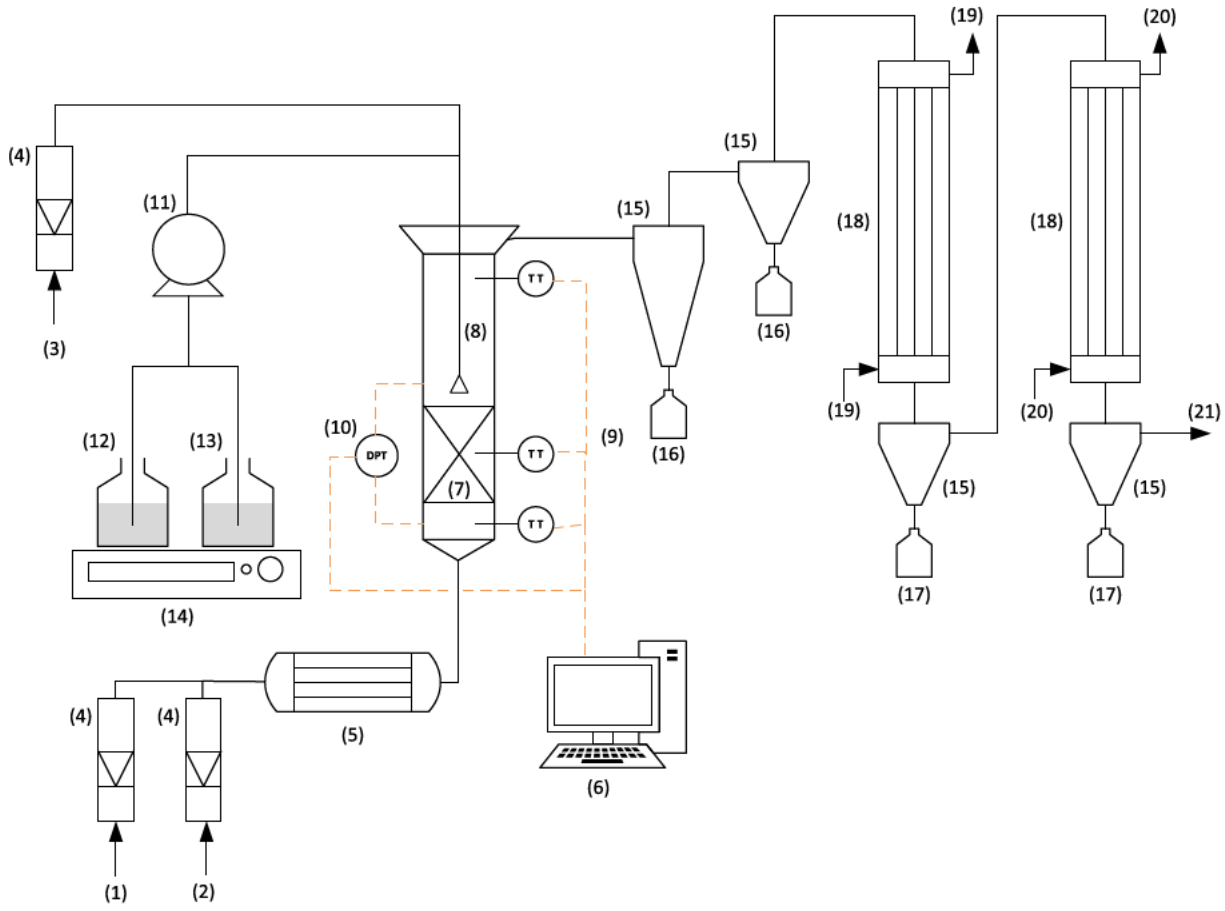

Fig. 1. Dry impregnation process: 1, air inlet; 2, N_2 inlet; 3, atomizing gas inlet (air or N_2); 4, rotameters; 5, heater; 6, PID regulation and acquisition system; 7, fluidized bed; 8, spraying system; 9, temperature sensors; 10, differential pressure sensor; 11, volumetric pump; 12, solvent tank; 13, precursor solution tank; 14, precision balance; 15, cyclones; 16, fine particle collectors; 17, solvent recovery containers; 18, condensers; 19, cooling water inlet/outlet; 20, aqueous solution of propylene glycol inlet/outlet; 21, dry gas vent.

DI of porous particles (alumina and silica) with aqueous salt solu tions [26,28,34] have shown that when the bed temperature is low ($T \leq 323$ K), the precursor is deposited essentially inside the pore volume, as the particles do not grow (i.e. are not coated) and the particle bed does not expand. Particle growth does not take place until the internal pores are completely filled.

Once the set point temperature is stable, the feed gas stream is switched from air to N_2. In order to reduce the thermal perturba tion caused by the liquid atomization, pure solvent is initially sprayed into the column at the same flow rate as the precursor solution. Note that this step causes the temperature of the bed to decrease slightly. When the temperature returns to the set point value, the pure solvent is replaced by the precursor solution. At this point, the bed is intermittently sprayed (10 s of spraying and 20 s of drying) with HQ solution for as long as is necessary to obtain the desired precursor content (i.e. ratio of the mass of impregnated precursor to the mass of the support material used). The pulverized solution penetrates the porous support by capillarity (liquid spreading and penetration kinetics), and at the same time, the sol vent evaporates owing to the thermal energy contributed by the fluidization gas (drying kinetics). These phenomena depend on: (i) the process related variables (fluidization gas flow rate, bed temperature, atomizing gas and liquid flow rates, and atomizer location), and (ii) the physicochemical properties (liquid interfacial tension, liquid viscosity, wettability, and nature and texture of the support material) [25 28]. So, the interdependency between these two families of parameters determines the product quality and the distribution of the precursor among the porous particles. Owing to these phenomena, if the external heat and mass transfer coeffi cients are low (i.e. low drying rate and slow evaporation of the sol vent), the liquid sprayed on the surface of the porous particles can migrate inside the support material before the drying causes pore plugging. These external heat and mass transfers depend both on the partial pressure of the solvent at the solid/gas interface and on the partial pressure in the fluidized bed. Under these conditions, rapid solvent evaporation is avoided when the drops and the solid particles are in contact.

To determine whether capillarity or drying is the dominant phenomenon, an impregnation index is defined as the ratio of the drying time to the capillary penetration time. The drying time is defined as the time needed by a particle saturated with pure sol vent to dry under fluidized bed conditions. The capillary penetra tion time is the time needed by the liquid to penetrate the pores. Distribution of the precursor can be considered as uniform when the impregnation module exceeds 11 [25,26].

Finally, at the end of the operations, spraying is stopped and the impregnated product is cooled before being removed by suction. A theoretical precursor content is calculated based on the ratio of the quantity of precursor sprayed to the mass of the porous particles initially present in the fluidized bed. The deposition efficiency is thus calculated based on the ratio of the experimental precursor content to the theoretical one.

2.2.3. Gas capture measurements

Gas capture measurements are performed by means of a gravi metric method using a Rubotherm magnetic suspension balance. The experimental apparatus detailed in Fig. 2, was initially adapted and used by Khaddour and coworkers [35] to monitor CH_4 adsorp tion on activated carbon. This apparatus consists of a jacketed magnetic suspension balance connected to a gas storage tank, and a vacuum pump that produces a primary vacuum of 0.1 kPa throughout the system. The temperature is measured by a Pt100 probe (with an accuracy of 0.1 K) placed directly in the measure ment chamber. The temperature is maintained at the desired value, with a stability of ±0.02 K, by continuous forced circulation of sili cone oil in the jacket using a thermostatic bath (Thermostat MPC

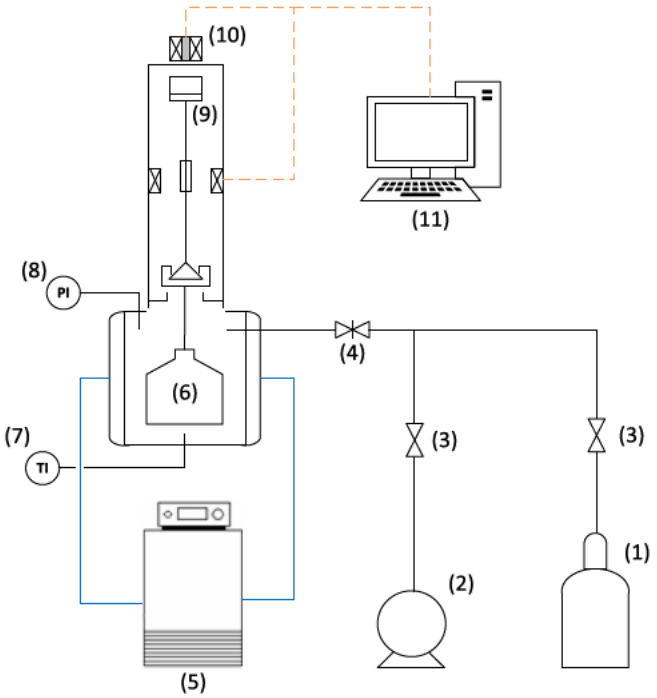

Fig. 2. Schematic diagram of the experimental apparatus for gas capture measure- ments: 1, gas tank; 2, vacuum pump; 3, plug valves; 4, fine adjustment valve; 5, thermostatic bath; 6, crucible; 7, temperature sensor; 8, pressure sensor; 9, permanent magnet; 10, electromagnet; 11, PID regulation and acquisition system.

K6, Huber). The pressure gauge (Wika) has a sensitivity of 0.01% of full scale.

The pure HQ is ground to a powder with a particle size of about 100 μm, to promote the gas solid reaction. The composite materi als are used immediately after they have been prepared. For the experiments, approximately 1 g of sample is placed into a stainless steel crucible directly in the measurement chamber. Prior to oper ations, the sample is purified at 323 K under vacuum until the mass is stable. The measuring principle based on the mechanical bal ance of forces acting on the system placed in the measurement chamber and the method are the same as described by Khaddour and coworkers [35]. A calibration step performed with He means that the accurate volume and mass of the sample before gas cap ture can be obtained. In this gravimetric method, the amount of gas captured is defined as an excess mass detailed in Eq. (1):

$$m_{excess} \quad m_{capt} \quad \rho_{gas} \cdot V_{capt} \tag{1}$$

where, m_{excess} is the excess mass, m_{capt} the total mass of gas cap tured, ρ_{gas} the gas density, and V_{capt} the total volume of gas cap tured. In this work, the excess mass is assumed to be equal to the total mass of CO_2 captured. As CO_2 HQ clathrates remain stable a few hours after they have formed at ambient conditions [21], this assumption (i.e. $m_{excess} = m_{capt}$) can easily be tested by comparing the data given by the suspension balance (obtained by a measure ment *in situ*) with a simple mass balance obtained by weighing the sample before and after the reaction using a conventional pre cision balance (precision of 1 mg). In an experiment in which 1.4 g of powdered HQ reacted with CO_2 at 3.0 MPa for 30 days at 25 °C, the mass difference between m_{excess} and m_{capt} was less than 0.1 %, which proves the validity of our assumption.

The CO_2 capture measurements are realized under the chosen conditions of 323 K and 3.0 MPa. The gas is admitted to the mea surement chamber from vacuum to 3.0 MPa, and the pressure is kept constant throughout the experiment by continuously adding feed gas. The CO_2 release step is performed by reducing the pres

sure in the system from 3.0 MPa to 0.1 kPa. This large pressure variation has a substantial impact on the temperature, and a period of about 10 min is necessary for the temperature to reach the target of 323 K again. During this transient period, the mass measurement is not reliable and it is impossible to identify the onset of the dissociation step. The conditions for gas capture (i.e. formation of the CO_2 HQ clathrates) and regeneration (i.e. dissociation of the CO_2 HQ clathrates) were determined based on the three phase equilibrium curve for the CO_2 HQ system [20]. The reproducibility of the experiments was tested on two different samples from the same batch of impregnated particles, both for clathrate formation and dissociation. The results obtained, i.e. the molar quantity of CO_2 captured during formation and released during dissociation versus time (up to 5000 min), demonstrate good reproducibility with an average relative error of around 7%.

2.3. Analytical techniques

The samples of composite materials taken at the end of each experiment are analyzed using different characterization techniques such as particle size distribution, scanning electron microscopy (SEM), energy dispersive X ray spectrometry (EDX), thermogravimetric analysis (TGA), differential scanning calorimetry (DSC), porosimetry, solid state ^{13}C NMR spectrometry, and X ray tomography. The technical details of these techniques can be found in the Supplementary Material.

3. Results and discussion

3.1. Characterization of composite materials prepared by DI

The series of experiments were conducted with large SF (H SF), small SF (L SF) and SS silica particles. No color change of the product was observed at the end of the operation (i.e. the impregnated particles were totally white), which suggests that the HQ did not undergo any chemical transformation (e.g. oxidation).

In order to confirm the nature of the deposit, samples of impregnated H SF, L SF and SS silica particles were analyzed by TGA/DSC. As an example, the TGA/DSC curves for impregnated H SF particles are shown in Fig. 3. For all three types of impregnated particles, the DSC curves showed three regions of interest: between 293 and 413 K (from point A to B), between 433 and 473 K (from point B to C), and above 473 K (point C to D), corresponding to the vaporization of the residual ethanol, the sublimation and fusion of the HQ, and the degradation and volatilization of the residual molten HQ, respectively. These observations confirmed other results reported previously in literature which demonstrated that HQ sublimes readily at a temperature lower than its melting point [36], and that it degrades at high temperature after its melting point (445 ± 0.6 K from the NIST) [37,38]. A

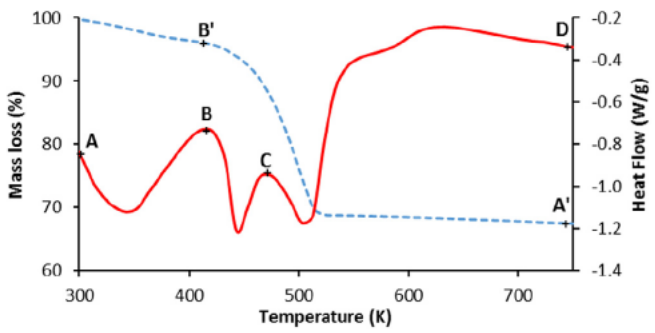

Fig. 3. TGA (dashed line) and DSC (full line) analysis of impregnated H-SF particles.

DSC analysis performed on pure HQ revealed the presence of two endothermic peaks only which is consistent with data from literature [38].

In addition, the impregnated particles were analyzed by ^{13}C NMR spectrometry. Spectra collected for all samples revealed two groups of signals at 116 and 148 ppm. An example of a spectrum obtained for impregnated H SF particles is shown in Fig. 4. These chemical shifts, attributed to non substituted and hydroxyl substituted carbons respectively, are in perfect agreement with the chemical shifts observed for pure HQ [21]. Based on the results of the DSC and ^{13}C NMR analyses, we were consequently able to demonstrate that the deposit is pure HQ.

The precursor content was determined from the evolution of the weight of the sample versus temperature (i.e. the TGA curve shown in Fig. 3) using Eq. (2):

$$\tau_{real} \quad 100\frac{W_f}{100}\frac{W_i}{W_f} \tag{2}$$

where W_f is the percentage of total weight loss (Fig. 3 point A′), and W_i the percentage of weight loss corresponding to the evaporation of ethanol (point B′).

The HQ contents obtained were therefore 0.37, 0.19 and 0.44 $g^{HQ}/g^{Support}$ for the H SF, L SF and SS particles respectively. As expected, the deposition efficiency with DI was greater than 0.9 for the silica particles, as the theoretical HQ contents were 0.38, 0.19, 0.50 $g^{HQ}/g^{Support}$ for the H SF, L SF and SS particles respectively. To assess the impact of particle size on this result, the impregnated batch of H SF particles was divided into three size classes by sieving: 500 μm < d < 560 μm; 560 μm < d < 800 μm; 800 μm < d < 1000 μm. The precursor content of each size class was then determined by TGA/DSC analysis. The results showed that the relative error as regards the uniformity of HQ distribution in the batch of particles did not exceed 2%.

In order to analyze how HQ is deposited in the porous material during the impregnation experiments, samples were taken at different times and analyzed by TGA/DSC. Note that the qualitative distribution analysis of HQ on the cross section of the impregnated particles was performed solely on impregnated H SF particles, as they were the only ones large enough to be cut with a scalpel. Samples corresponding to 0.10, 0.18, 0.19, 0.22 and 0.37 $g^{HQ}/g^{Support}$ were collected, and SEM observations coupled to EDX analyses of the surface and cross section of these samples were then performed to determine the threshold above which impregnation took place on the surface. To calculate the precursor content at a given position on the particle cross section, the atomic percentages of the main elements (silicon, oxygen, and carbon) were determined by EDX spectroscopic analysis. Based on these data, it was then easy to calculate the precursor content, assuming that one atom of silicon is equivalent to one molecule of silica (the chemical formula of silicon dioxide is SiO_2) and that one molecule of HQ contains six carbon atoms (the chemical formula of HQ is $C_6H_6O_2$). For example, Fig. 5 shows the different places where EDX analyses were run, from the center to the external surface of a particle impregnated at 0.37 $g^{HQ}/g^{Support}$. From these analysis, the radial distribution of the HQ in the impregnated particles for different precursor contents can be estimated, and the results are plotted in Fig. 6.

In Fig. 6, when the ratio r:R (i.e. the distance r from the center to the maximum limit radius R) is close to 1, this means that the distance r from the center of the particle is close to the maximum limit radius R. In addition, an HQ mass fraction of $w^{HQ} = 1$ in Fig. 6 indicates that the solid measured by the EDX probe is pure HQ. For a ratio r:R of less than 0.8, the HQ mass fraction observed was always about 28 wt%, corresponding to 0.22 $g^{HQ}/g^{Support}$. Interestingly enough, for the particles with a precursor content of 0.22

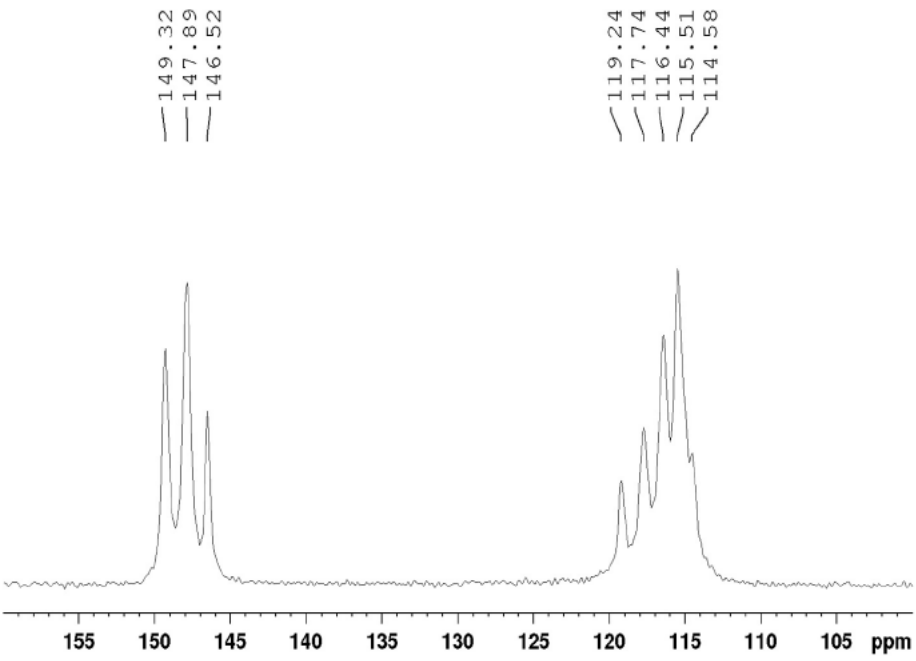

Fig. 4. ^{13}C NMR spectrum of impregnated H-SF particles.

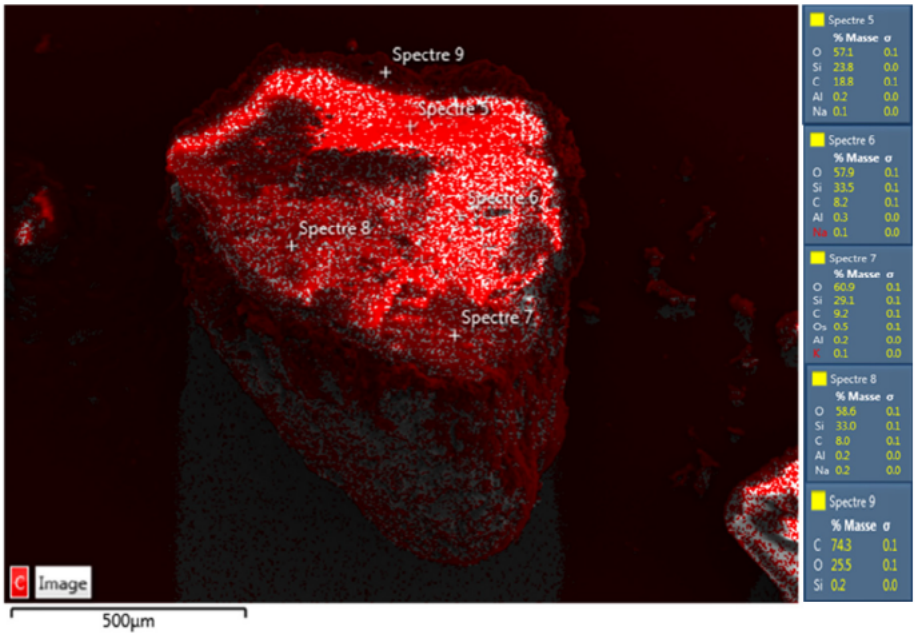

Fig. 5. EDX spectroscopic analysis on the cross-section of an H-SF particle impregnated at 0.37 $g^{HQ}/g^{Support}$. The red color shows the presence of carbon atoms.

and 0.37 $g^{HQ}/g^{Support}$, the mass fraction of HQ measured by EDX drastically increased to $w^{HQ} = 1$ for r:R = 1, meaning that an HQ crust had formed on the surface of the particle. From these measurements, we could therefore conclude that the impregnation took place on the surface above a precursor content threshold of 0.22 $g^{HQ}/g^{Support}$. However, SEM images showed, more precisely, that HQ molecules started being deposited on the particle surfaces from a lower precursor content, equal to 0.18 ± 0.01 $g^{HQ}/g^{Support}$ (see Fig. 7). The difference between the SEM observations (0.22 $g^{HQ}/g^{Support}$) and the EDX measurements (0.18 ± 0.01 $g^{HQ}/g^{Support}$) is consistent with the uncertainty of the method due to the carbon content observed for native silica particles. We can therefore conclude that HQ was deposited in the pores of SF particles when the precursor content was below 0.18 $g^{HQ}/g^{Support}$.

In addition, based on the pore volume of native H SF particles and the density of HQ (i.e. 1.33 g/cm^3), if all the pores were completely filled with HQ and no HQ was present at the surface, the maximum quantity of HQ inside the porous particle would be 1.7 $g^{HQ}/g^{Support}$. The real precursor content value obtained experimentally by TGA and EDX analysis (i.e. average value of 0.18 ± 0.01 $g^{HQ}/g^{Support}$) was found to be much lower than this hypothetical limit of 1.7 $g^{HQ}/g^{Support}$. This difference is explained by partial filling of the pore with HQ nanocrystal stacks. In this case, when the pores are partially filled with HQ nanocrystals, deposition occurs mainly on the external surface.

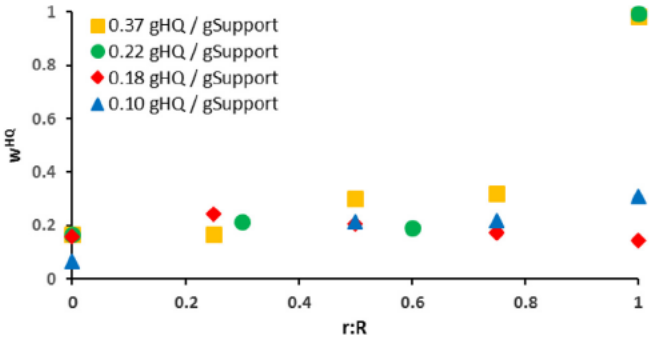

Fig. 6. Radial distribution of the HQ in H-SF particles impregnated at (▲) 0.10, (◆) 0.18, (●) 0.22 and (■) 0.37 $g^{HQ}/g^{Support}$. The ratio r:R is the distance r from the center to the maximum limit radius R.

Concerning the SS particles, only four samples, corresponding to 0.07, 0.17, 0.26 and 0.44 $g^{HQ}/g^{Support}$, were taken during the impregnation process. As indicated in the section above, the cross sections of these particles were not analyzed as the particles were too small to be cut properly with a scalpel. In this case, the first sample collected (containing 0.07 $g^{HQ}/g^{Support}$) showed that an HQ crust had already formed on the SS particles. Accordingly, the HQ content threshold above which the HQ deposition occurs on the external surface could not be precisely estimated for SS particles. We can only conclude that this value would be lower than 0.07 $g^{HQ}/g^{Support}$, and that this value is lower than the one found for SF particles (0.18 ± 0.01 $g^{HQ}/g^{Support}$). This difference can be explained by the drop in capillary pressure caused by the increase in the average pore diameter (the pore diameters for H SF and SS particles are approx. 33 and 99 nm respectively).

The morphology of the final product obtained with H SF and SS particles at the end of the impregnation process is shown in more detail in Fig. 8 (using SEM) and Fig. 9 (using X ray tomography). Pictures of the native supports (before impregnation) are available in the Supplementary Material. In Fig. 8c (showing impregnated H SF particles), the thickness of the HQ layer can be evaluated at around 36 μm. Moreover, it appears clearly that this layer is totally perforated.

Additionally, X ray tomography measurements were taken on impregnated H SF and SS particles (Fig. 9). These measurements confirmed that both particle types had a layer of HQ, but the texture and thickness of these layers were very different. As shown in the SEM analysis, the H SF particles presented a highly perforated HQ layer. X ray analysis showed that the layer thickness varied between ~5 and ~50 μm. In contrast, SS particles were uniformly coated, with an HQ layer of 14 ± 4 μm thick. The X ray data also revealed that HQ can migrate inside the particles and crystallize locally. This phenomenon can be clearly seen in Fig. 9d (H SF) and to a lesser extent in Fig.9h (SS). In order to estimate the amount of HQ in the nm sized pores, below the resolution of the X ray scan, the grey scale of the native and coated particles was analyzed and compared. Differences suggesting HQ impregnation were observed, but they are statistically not significant, and therefore do not provide conclusive evidence.

To characterize the porosity of our composite material, gas porosimetry experiments were performed. First of all, we observed in a preliminary test that the quantity of N_2 adsorbed on pure powdered HQ (particle size of about 100 μm) was negligible compared to that adsorbed on native silica. This observation revealed that HQ powder is not a mesoporous/microporous material. However, the specific area of HQ nanocrystals in the pores cannot be overlooked, as their maximum diameter would be limited by the pore size of native SF particles (i.e. around 38 nm). The measured adsorption and desorption isotherms of N_2 gas at 77 K are presented in Fig. 10 for native and impregnated SF particles. The isotherms are type IV, according to the IUPAC nomenclature [39], with hysteresis loops of type H1 indicative of mesoporous materials with a cylindrical pore shape. In this case, N_2 capillary condensation occurred in the pores.

The cumulative pore volume and the PSD for the desorption branch are shown in Fig. 11. Based on the PSD of impregnated SF particles, two distinct pore size classes were found: (i) the first was fully consistent with the pore diameter measured for native SF particles (i.e. 38 ± 5 nm), and corresponded to around 51% of the pore volume of the composite material; and (ii) the second class, centered on 20 nm, corresponded to the remaining pore volume (i.e. 49%). Accordingly, we concluded that about half of the pores (i.e. ~51%) were HQ free and that the balanced pores were partially filled with HQ nanocrystals. On the basis of this analysis, the pore volume and specific area were determined as being 0.53 cm^3/g^{sample} and 81 m^2/g^{sample} respectively. In light of these values, it was clear that the HQ layer observed in the SEM images (see Fig. 8) was totally permeable to gases such as N_2. In comparison, the porous volume and the specific area of native SF particles were 0.89 cm^3/g^{sample} and 144 m^2/g^{sample} (see Supplementary Material Table SI1). Consequently, as both the pore volume and specific area decreased after the impregnation step, it could be concluded that the textural parameters of the native particle were significantly

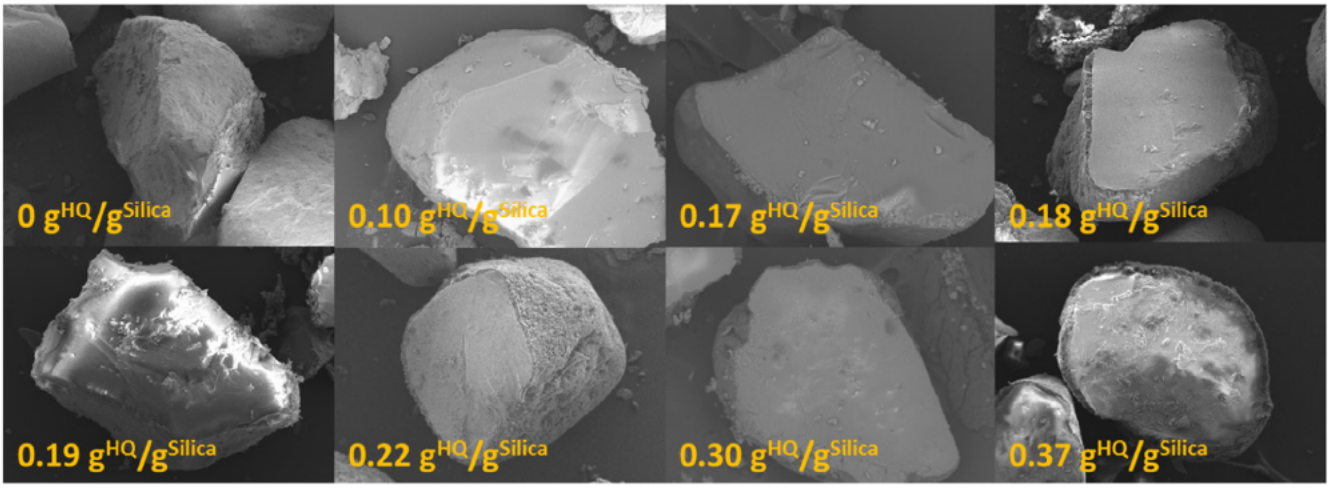

Fig. 7. SEM images of the cross-section of dry-impregnated H-SF particles collected at different times during the impregnation experiment.

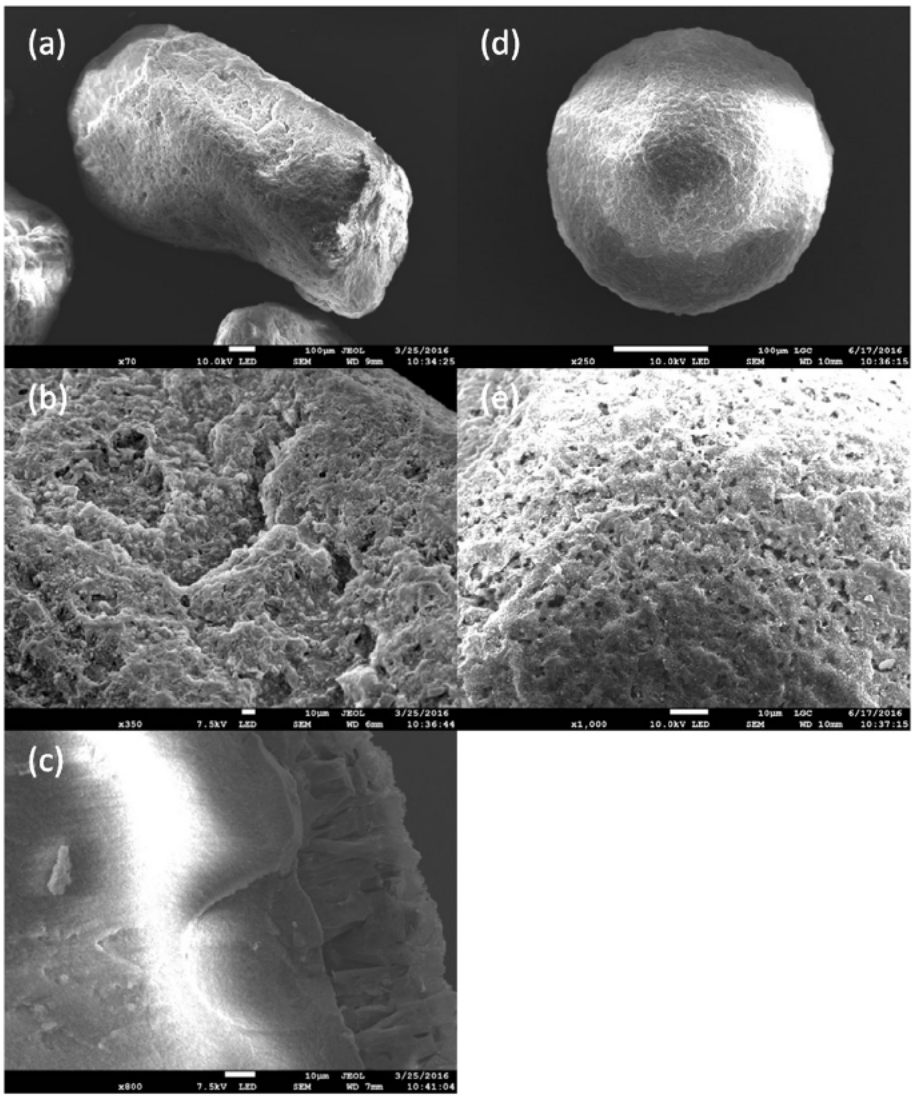

Fig. 8. SEM images of H-SF particles impregnated by DI at 0.37 $g^{HQ}/g^{Support}$: (a) full particle, (b) external surface, and (c) cross-section of the particle. SEM images of SS particles impregnated by DI at 0.44 $g^{HQ}/g^{Support}$: (d) full particle and (e) external surface.

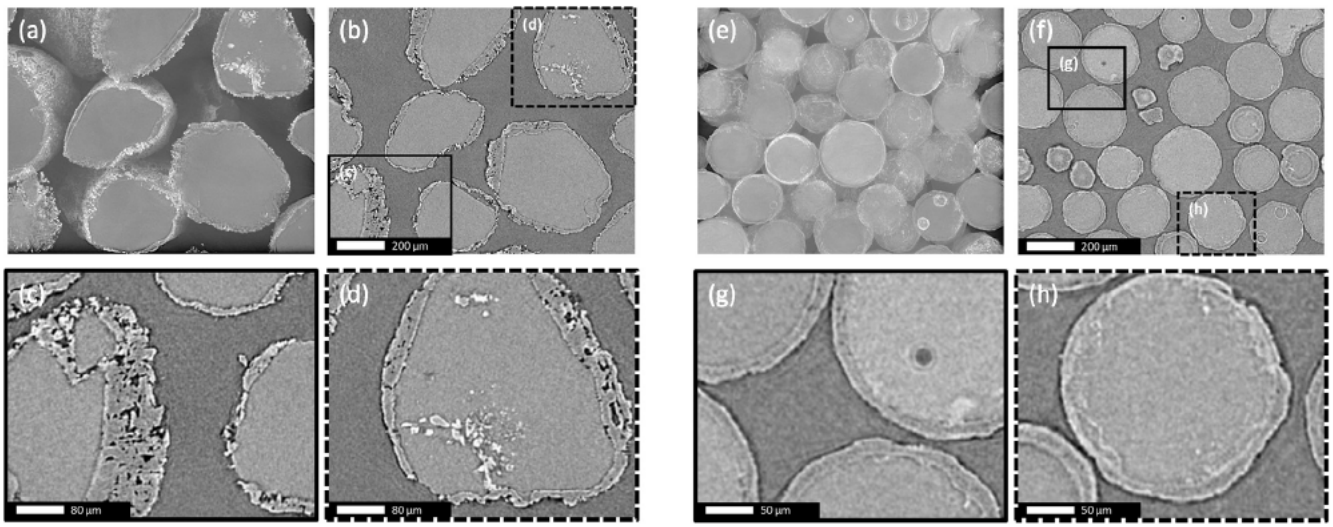

Fig. 9. X-ray tomography of dry-impregnated H-SF and SS particles: (a, e) 3D reconstructions, (b, f) slice of the particle stack, and (c, d, g, h) close-up views of regions of specific interest.

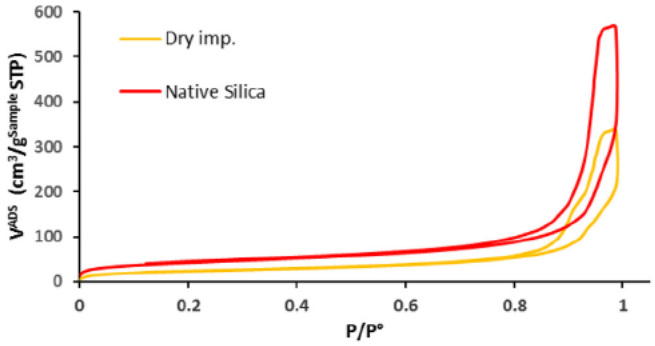

Fig. 10. N_2 adsorption–desorption isotherms at 77 K: impregnated SF particles (yellow line) and native SF particles (red line).

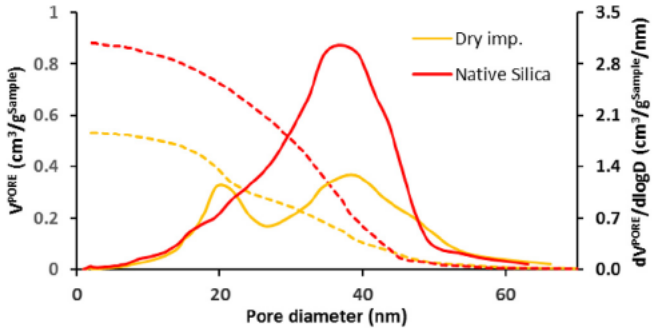

Fig. 11. Pore size distribution (full line) and cumulative pore volume (dashed line) function of pore diameter: impregnated SF particles (yellow) and native SF particles (red).

modified by the impregnation process. The 40% decrease in pore volume (with respect to native particles) could be attributed to the presence of the HQ impregnated in the pores. The loss of 44% of the specific area could be ascribed to the fraction of the silica surface covered by the HQ nanocrystals impregnated in the pores. However, the variation in the pore volume and specific area was also due to the increase in sample mass (which also comprised the HQ impregnated on the external surface) making it impossible to adequately elucidate the situation.

As the impregnation took place in the pores as well as on the surface of the H SF and SS silica particles, the adhesion of the deposit was evaluated by a 3 h attrition test. Fig. 12 shows SEM images of impregnated SS before and after the attrition test. After this test, the particles were visualized by SEM and their precursor content was determined by TGA. The almost identical precursor content values obtained, with a relative difference of 2% and simi lar product morphologies before and after the attrition test, were proof that the HQ layer adhered very well on the particle surface.

3.2. Characterization of composite materials prepared by WI

Despite the large size dispersion of SF particles, particles were not separated by size as there were no operating constraints related to this factor. The characterization results of WI were com pared to those obtained by DI. First of all, TGA was used to deter mine the precursor contents of the SF and SS particles 0.44 and 0.36 $g^{HQ}/g^{Support}$ respectively. The DSC profiles confirmed the pres ence of HQ. Furthermore, it appeared that wet impregnated SF par ticles were more impregnated by HQ than SS particles. Fig. 13 shows SEM images of the final impregnated SF and SS particles. We observed that the surfaces of both type of particles were cov ered with HQ crystals, which were larger in the case of impreg nated SS particles than of impregnated SF particles. Furthermore, the HQ crystals observed after WI seemed less smooth than those obtained by DI.

The SEM image of the cross section of wet impregnated SF par ticles (Fig. 13c) revealed a large perforated HQ layer of around 57 ± 17 μm, which is thicker than the layer observed for dry impregnated SF particles. Moreover, it seems that there are two different HQ layers: (i) a thick HQ layer in direct contact with the SF particle, and (ii) a thin layer composed of HQ crystals supported by the first HQ layer. Effectively, as the impregnation solution came into contact with the silica particles, the capillary forces caused the HQ solution to flow rapidly toward the particle surface. Ethanol diffused more readily than HQ in the particle pores because of the small size of ethanol molecules and their affinity for silica. This phenomenon led to a sharp increase in the concen tration of HQ near the surface and probably to a concentration gra dient inside the particles. The duration of the transfer of HQ inside the particle pores determined the HQ concentration profile there. This step was mainly controlled by the diffusion process, which depends on the molecular properties of the impregnation solution and the textural properties of the support material. After filtration, the drying step determined how HQ was distributed inside the pores [32,33]. This complex step combined crystallization and the drying operation performed in a confined environment. So, the crystallization kinetics depend on the average pore size [40]. The phenomenon of competition between drying and crystalliza tion led to: (i) migration of the solution from the ethanol rich zone (center of the particle) to the surface, and (ii) dissolution/recrystal lization of HQ at the surface. So, solvent evaporation and HQ crys tallization occurred essentially at the surface of the particle (at the pore entrances), justifying the presence of the HQ layers.

In the same way as for dry impregnated particles, X ray scans of wet impregnated H SF and SS particles were acquired (Fig. 14). The thickness of the layer coating the H SF particles was observed to be highly irregular, with some surfaces uncovered and others with layers of up to 80 μm or more, even on the same particle (e.g. Fig. 14c). In the case of SS particles, the X ray scans confirmed the deposition of HQ crystals on the surface as observed with the SEM. Additionally, significant impregnation inside the particles was detected. Generally speaking, the uniformity of impregnation is noticeably less good in the WI method compared to the DI method.

N_2 gas porosimetry experiments gave a specific area and total pore volume of about 79 m^2/g^{sample} and 0.46 cm^3/g^{sample} for wet impregnated SF particles. These results, very close to those obtained for dry impregnated SF particles, led to the same conclu sions: (i) the HQ layer present at the particle surface is permeable to gases, (ii) about 42% of pores are HQ free, and (iii) the balanced pores are partially filled with HQ.

3.3. Use of composite materials as reactive media for CO_2 capture

The objective of these experiments was to obtain both the gas storage capacity of the reactive medium and data on the CO_2 cap ture kinetics. For comparison purposes and so as to not to take into account the initial sample mass, the results are discussed as the ratio of the captured gas mass to either the mass of the support material or the mass of the impregnated HQ. The composite mate rials obtained by impregnating SF and SS particles with HQ are very similar, both in terms of HQ distribution inside and outside the particles and the properties of adhesion of the HQ to the silica. As discussed in the previous section, attrition tests performed with impregnated non spherical SF particles showed that the mechani cal resistance of this composite material is acceptable. In addition, for these experiments, SF particles are approximately 8 times less expensive than SS particles. As no major difference was in fact

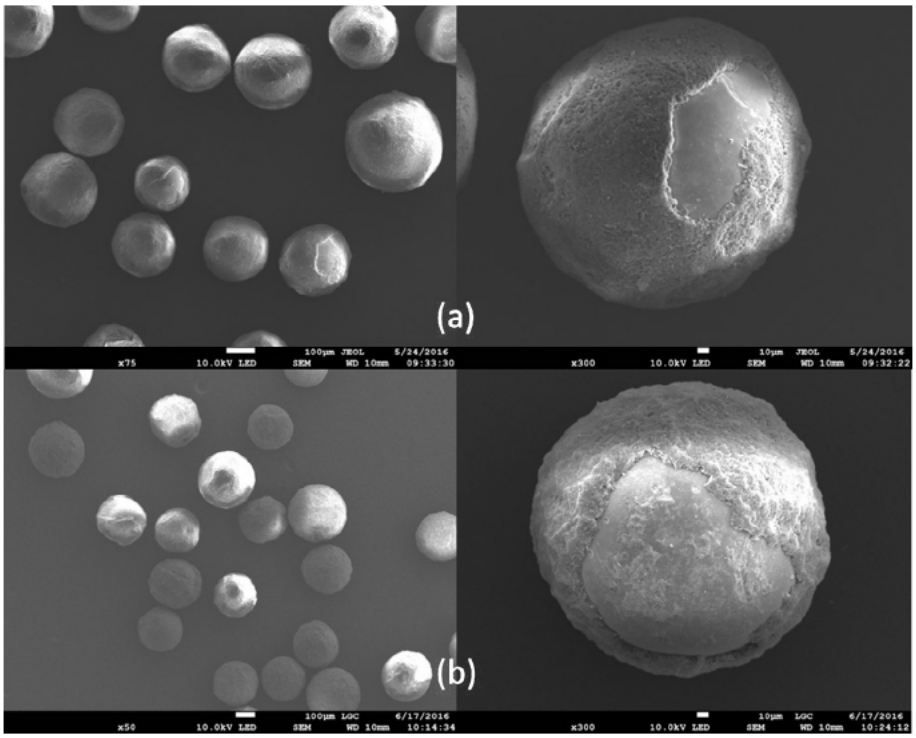

Fig. 12. SEM images of SS particles impregnated by DI at 0.44 $g^{HQ}/g^{Support}$: (a) before and (b) after the 3-h attrition test.

pointed out between the two types of particles after the impregnation step, the choice of SF is a reasonable option. Consequently, the composite material selected for our CO_2 capture experiments is the one based on SF particles. In order to compare and quantify the performances of this medium, pure powdered HQ and native SF particles are also evaluated in this section.

First of all, the result obtained for pure powdered HQ (see Fig. 15) revealed two different steps in the gas capture process, as already reported in literature [22]. The first small uptake (from point A) was attributed to CO_2 inclusion in the native HQ (α form) before the HQ clathrate (β form) formation: this phenomenon is called "solubilization in HQ α form" [1,41 43] as the α form has the same types of cavities as the HQ clathrates (the α form exhibits 1 cavity per 18 molecules of HQ, whereas the β form has 1 cavity per 3 molecules of HQ), and experimental evidence shows that sorption occurs within them [1,22,43]. The initial reaction rate for this phenomenon (point A') was determined as being 0.2 $mmol^{CO2}/kg^{HQ}/min$. An "induction time", corresponding to the time during which the native HQ starts to transform into clathrates (i.e. the β form), could thus be defined. This parameter was deduced from the enclathration rate values, calculated by numerical derivation from the quantity of CO_2 captured versus time (see the dashed curve in Fig. 15). We observed that the enclathration rate versus time curve passed through a minimum at point B'. This minimum is compatible with the two phenomena discussed taking place in succession (i.e. gas solubilization in α form and gas enclathration in β form). We therefore postulated that the second, larger, uptake (which begins at point B in Fig. 15) is ascribed to the enclathration phenomenon itself, as already proposed by Allison and Barrer (note that they did not provide any information on the method used to determine this parameter) [22]. At this point, the induction time could be determined as lasting around 254 min. 0.5 $mmol^{CO2}/kg^{HQ}/min$ is the maximum reaction rate (at point C') calculated during the second CO_2 uptake and 9.1 days (this time is not shown in Fig. 15 as the time axis has been truncated at 3600 min) is the characteristic time in which the clathrate occupancy (i.e. the proportion of cavities filled by the gas, ranging from 0 to 1 when the clathrates are guest free or when every cages are occupied, respectively [44]) is 50% (called t_c^{50}).

The general HQ clathrate formula is xG 3HQ, where G is the guest molecule and x the clathrate occupancy. In the case of ideal stoichiometry, the clathrate occupancy is expected to be equal to unity (i.e. 1 guest molecule per 3 HQ molecules) [44]. Nevertheless, it is worth noting that gas clathrate structures are often non stoichiometric (i.e. $x < 1$), which gives rise to a variable quantity of empty cages in the structure [21]. Considering the gas storage capacity of pure HQ, our experiment showed a negligible variation of mass versus time after 45 days of reaction. At this point, the gas storage capacity measured was 2.30 mol^{CO2}/kg^{HQ}, which corresponds to a clathrate occupancy of 0.76. This value is in perfect agreement with literature data [14,21,30,38,45], and confirms that the system had reached a pseudo equilibrium state.

Both types of impregnated particles obtained by DI and WI were then tested as reactive media. The results of the quantity of CO_2 captured versus time obtained with these particles are presented in Fig. 16, and compared to those obtained using pure powdered HQ or native SF particles. Interestingly enough, at the end of the experiments carried out with the composite materials (after about 3600 min of reaction) if only the gas enclathration phenomenon is considered the calculation gives improbable clathrate occupancy values: x equals 1.96 and 1.64 for dry and wet impregnated particles respectively. Note that for pure HQ, the clathrate occupancy was 0.29 after 3600 min of reaction. As it was demonstrated previously that the CO_2 HQ clathrate cavity can accommodate only one CO_2 molecule at the most [21], we were able to conclude that the gas storage capacities obtained by using these two types of reactive media cannot be explained by considering just one enclathration phenomenon. In addition, the amount of CO_2 adsorbed on the native silica is non negligible (i.e. 1.2 mol^{CO2}/kg^{Sample}) compared to the total quantity of CO_2 captured by the impregnated particles (i.e. 1.60 and 1.53 mol^{CO2}/kg^{Sample} for dry and wet impregnated particles respectively).

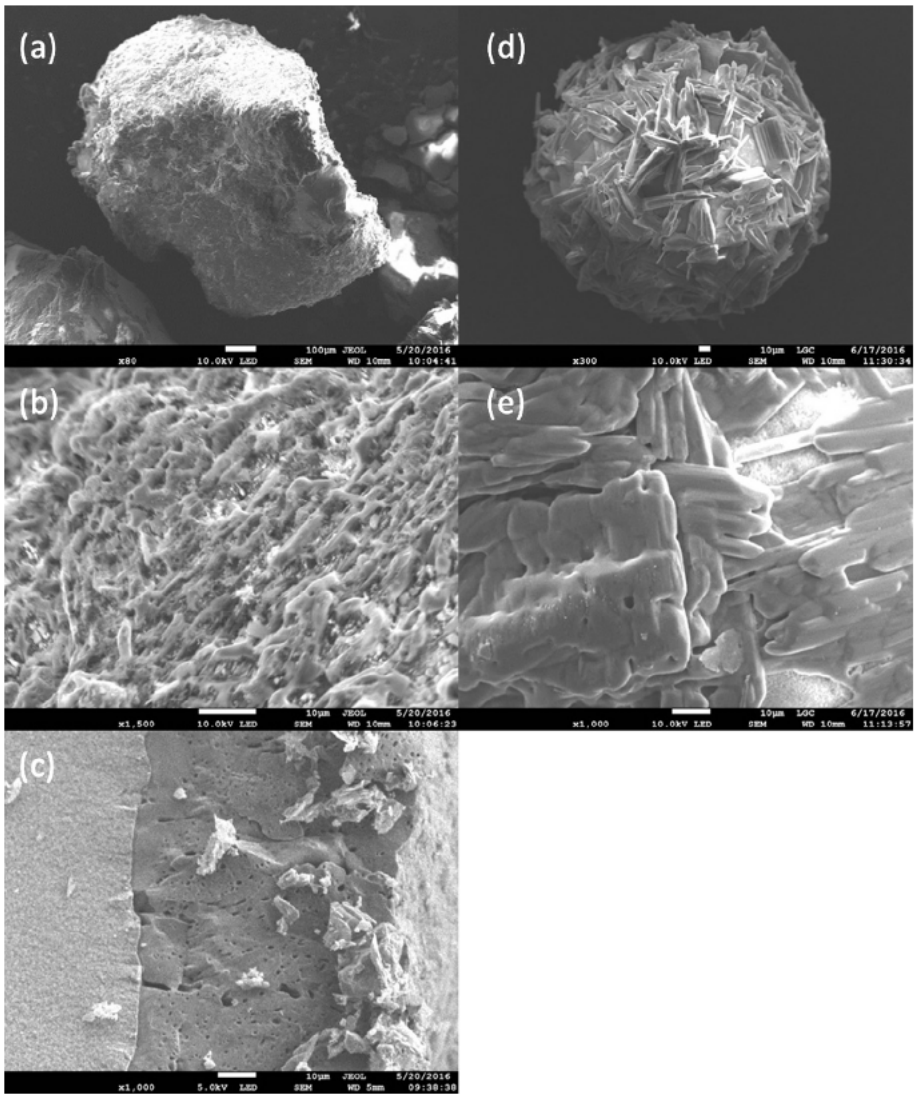

Fig. 13. SEM images of SF particles impregnated by WI at 0.44 $g^{HQ}/g^{Support}$: (a) full particle, (b) external surface, and (c) cross-section of the particle. SEM images of SS particles impregnated by WI at 0.36 $g^{HQ}/g^{Support}$: (d) full particle and (e) external surface.

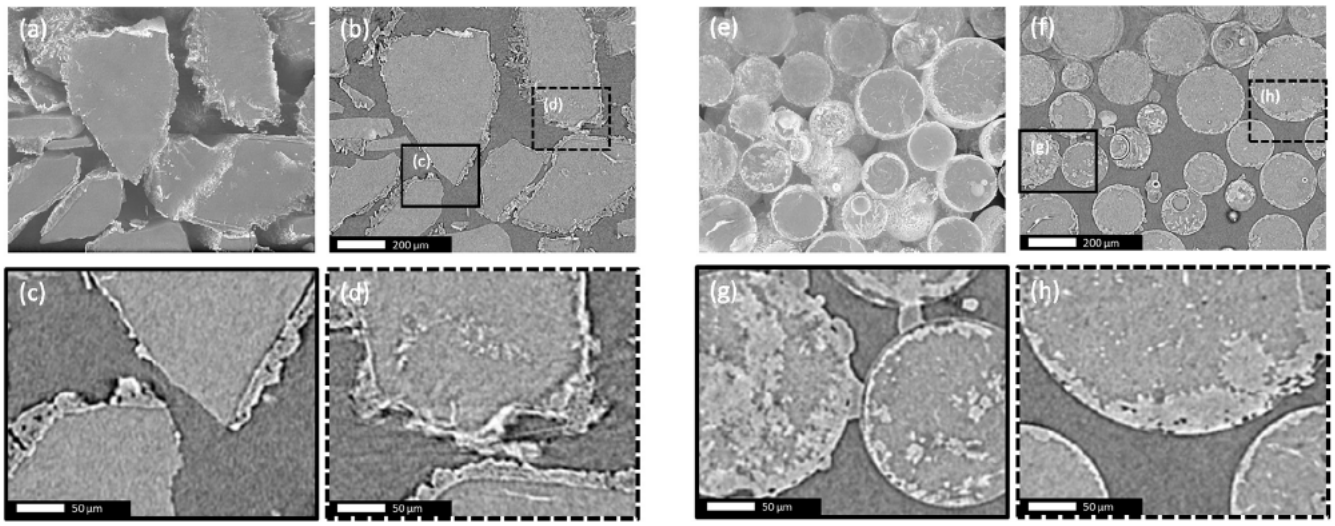

Fig. 14. X-ray tomography of wet-impregnated H-SF and SS particles: (a, e) 3D reconstructions, (b, f) slice of the particle stack, and (c, d, g, h) close-up views of regions of specific interest.

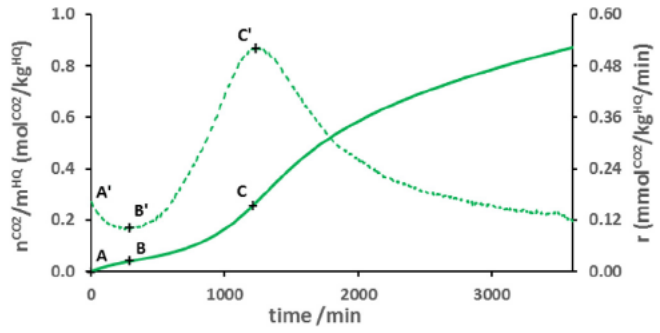

Fig. 15. Quantity of CO_2 captured by pure HQ function of time: storage capacity (full line) and reaction rate (dashed line) at 3.0 MPa and 323 K.

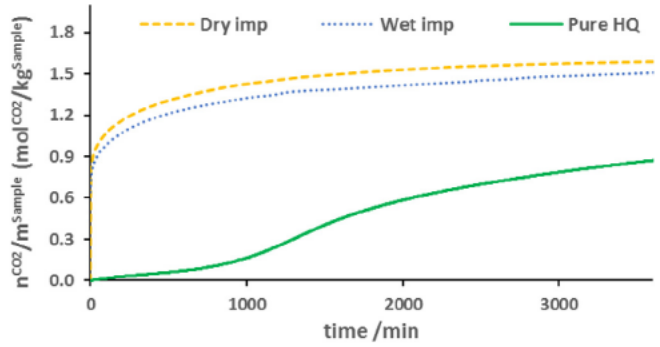

Fig. 16. CO_2 capture experiments at 3.0 MPa and 323 K: molar quantity of captured CO_2 normalized by sample mass function of time: pure powdered HQ (green full line), reactive media prepared by DI (yellow dashed line), reactive media prepared by WI (blue dotted line), and native SF particles (red dashed line).

Moreover, the kinetics of CO_2 adsorption on the native silica are much faster than the global kinetics of CO_2 capture with the composite materials, as the time needed to reach the equilibrium value is 6 ± 3 min for the native silica against at least 2 days for the impregnated particles. It can therefore be inferred that the media as synthesized allow both CO_2 adsorption on the reactive media and CO_2 enclathration through CO_2 HQ clathrate formation.

Considering that the adsorption on silica takes 6 ± 3 min, the quantity of gas captured by adsorption can be estimated from the graph at 0.84 ± 0.04 and 0.77 ± 0.04 mol^{CO2}/kg^{Sample} for dry and wet impregnated particles respectively. The difference observed between the adsorption capacity of impregnated particles and native silica is in line with the decrease in specific area observed in the porosimetry analysis (i.e. from 144 m^2/g^{sample} for native silica to 81 and 79 m^2/g^{sample} for dry and wet impregnated particles respectively). It is worth noting that when dry impregnated particles were used instead of wet impregnated ones, the quantity of CO_2 adsorbed increased by 8%. The quantity of CO_2 likely to be trapped in HQ clathrates can be calculated by deducting these adsorption capacities from the total amount of CO_2 gas captured. It appears that the enclathration capacities are 2.81 ± 0.15 and 2.49 ± 0.15 mol^{CO2}/kg^{HQ} (corresponding to clathrate occupancies of x = 0.93 ± 0.05 and x = 0.82 ± 0.05) for dry and wet impregnated particles respectively, after a reaction time of about 3600 min. In light of these adsorption and enclathration capacities, it can be deduced that the impregnation technique has a direct impact on the efficiency of CO_2 capture in this type of composite material. Consequently, this type of composite material combines the effects of both adsorption and enclathration. Remember that the main aim of this study, however, was to enhance the enclathration reaction kinetics.

To follow the CO_2 capture kinetics due to the enclathration reaction only, the amount of CO_2 likely to be adsorbed was deducted from the total volume of CO_2 gas captured. Fig. 17 shows the amount of CO_2 gas captured by enclathration only as a function of time. For both dry and wet impregnated reactive media, it appeared that the CO_2 capture kinetics were much faster than for pure powdered HQ, and no induction period was measured. The initial reaction rates and t_c^{50} were 22 ± 6 $mmol^{CO2}/kg^{HQ}/min$ (t_c^{50} = 6.0 ± 1.5 h) and 19 ± 6 $mmol^{CO2}/kg^{HQ}/min$ (t_c^{50} = 9.6 ± 2.3 h) for dry and wet impregnated media respectively. It seems that whatever the impregnation technique, the enclathration kinetics were not affected, as both the initial reaction rates and t_c^{50} were very close to together for both dry and wet impregnated media. However, if the indicators obtained for dry impregnated particles are compared to those of pure HQ, we can see that the use of reactive media can significantly improve the enclathration kinetics: the initial reaction rate is multiplied by a factor of 44 with no induction period, and the t_c^{50} is divided by a factor of 37 (with respect to pure HQ). We believe that both the improved enclathration kinetics and the drastic reduction in the induction time observed when impregnated particles are used instead of native HQ are mainly due to the large increase in the reactive surface area between the HQ and the gas. This effect, observed when ground HQ is used, had already been pointed out in literature [14,15,22], but the experimental evidence was insufficient. However, complementary tests for different P/T conditions using composites with different HQ contents will need to be performed to properly quantify how the kinetics and the adsorption are affected by the amount of HQ loaded, the thickness of the HQ layer and the operating conditions.

Fig. 18 presents the results obtained for two successive cycles (one cycle being a formation step followed by a regeneration step). Several experiments were performed (until four successive formation/dissociation steps were completed) with different composite materials, and the tendencies observed and discussed below demonstrate good reproducibility (only two runs are plotted in Fig. 15 for the sake of clarity). After the first reaction step, the reactive media were regenerated by depressurizing and evacuating the system. As observed in Fig. 18b, the CO_2 was released in two distinct steps, which was attributed to the successive release of CO_2 adsorbed on the reactive media and the dissociation of the CO_2 HQ clathrates previously formed. Note that desorption was faster than the clathrate dissociation, which is consistent with our previous conclusions. Now looking at Fig. 18a, the second gas capture run made on a regenerated particle confirmed that the as synthesized media could reversibly capture the CO_2. The capture kinetics during the second reaction step were quite similar, as the initial reaction rate was 28 ± 14 $mmol^{CO2}/kg^{HQ}/min$ and the t_c^{50} was 10.2 ± 5.0 h (instead of 22 ± 6 $mmol^{CO2}/kg^{HQ}/min$ and t_c^{50} = 6.0 ± 1.5 h for the first formation). On the contrary, the gas

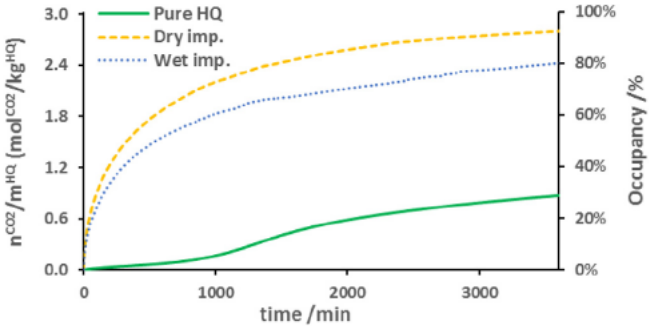

Fig. 17. Amount of CO_2 captured by enclathration (at 3.0 MPa and 323 K) normalized by mass of impregnated HQ function of time: pure powdered HQ (full line), and reactive media prepared by DI (dashed line) and by WI (dotted line).

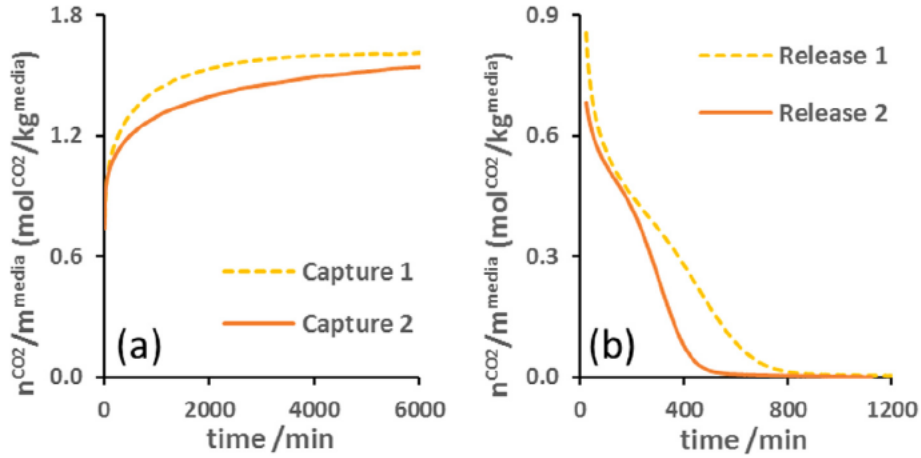

Fig. 18. CO_2 capture (a) and release (b) normalized by mass of the media (impregnated SF particles) function of time: first (dashed line) and second (full line) run of CO_2 capture/release.

release kinetics measured for the second dissociation run (Fig. 18b) were faster than in the first step. Indeed, the time needed to remove all the CO_2 captured by the media decreased from 844 to 575 min. We currently have no clear explanation as to why the gas capture and release kinetics differed from the first step to the second. HQ structuration (e.g. combination or agglomeration of nanocrystals) might have well occurred inside the pores of the HQ during the first clathrate formation, which could have caused a decrease in the CO_2/HQ contact area and modified the diffusion of the gaseous species inside the crystal. The complete mecha nisms could be explained in depth if some additional *in situ* spec troscopic measurements were performed (for example, ^{13}C NMR and Raman spectroscopy). Thanks to complementary experiments such as these, it should be possible to identify the different states of the captured CO_2 molecules (in the hydroquinone clathrates and adsorbed on the material's surface). The main difficulty in car rying out this type of *in situ* measurement is to develop analytical devices and robust techniques that function under relatively high pressure and temperature conditions, and are able to give reliable information as regards what is happening inside the pores of the composite materials. These points are currently being developed in our laboratory.

4. Conclusions

This study is devoted to the development of composite materi als that can be used as reactive media for CO_2 capture by hydro quinone clathrates. The use of ground HQ (i.e. HQ powder) for the enclathration reaction seems incompatible with industrial applications because of the excessively long reaction time and the process and safety issues related to the use of raw pulverulent material. The composites developed and tested in this study are made of HQ supported on two types of porous silica particles (Sil iasphere® and Siliaflash®) from Sillicyle. Two techniques were used for the impregnation with HQ: dry impregnation (DI) in a fluidized bed and wet impregnation (WI). For the two types of silica particles and impregnation techniques used, the results in terms of HQ loca tion and dispersion, morphology of the impregnated particles, and HQ content obtained were almost identical. Various analyses, par ticularly DSC and ^{13}C NMR, demonstrated that there was no chem ical modification of the HQ structure after its impregnation on silica particles. The SEM and tomographic images revealed that the silica particles are coated with a thick, perforated HQ layer and that there the HQ adheres well on the silica surface. These observations imply that support precursor chemical interactions are important and necessary for an efficient impregnation with HQ. Porosimetry analysis of the impregnated particles revealed that about half of the pores are HQ free and that the balanced pores are partially filled with HQ nanocrystals, resulting in a decrease of the pore volume and of the specific area compared to that of the native particles. The high availability of the silica sur face confirmed that the HQ layer is permeable to gas molecules. These last observations suggest that the as synthesized silica HQ reactive media allow coupling of adsorption/enclathration phenomena.

The CO_2 capture measurements performed at 323 K and 3.0 MPa with a magnetic suspension balance demonstrated that the particles impregnated by HQ clathrates significantly enhance the kinetics of CO_2 capture compared to powdered HQ. In addition, the choice of impregnation technique plays an important role on the global efficiency of this type of reactive media due to possibil ity of additional CO_2 adsorption. DI could therefore be preferred to WI. Because the composite material offers a large HQ surface area for the gas/solid reaction and is relatively easy to handle, it was found to present a number of advantages compared to pure pow dered HQ: (i) no induction period is needed to start the CO_2 cap ture, (ii) the initial reaction rate increases by a factor of 44 if dry impregnated particles are used, (iii) the time needed to fill 50% of the cavities inside the structure decreases by a factor of 37 compared to pure powdered HQ, and (iv) the test on two forma tion/regeneration cycles shows that this process is reversible. Additional tests need to be run for different P/T conditions using composites with different HQ contents to measure how the enclathration kinetics and adsorption are affected. Although the enclathration kinetics were greatly enhanced by using particles instead of powdered HQ, we are aware that this study, carried out in static conditions at one working pressure and temperature, is just a first step in demonstrating the potentiality of a composite material of this type. Now, the reactive media has to be tested in a real gas/solid contactor (fixed or fluidized bed) at different pres sures, temperatures, gas compositions and flow rates to evaluate whether the reaction time can be reduced to an acceptable level suitable for industrial applications. Finally, we noticed that the first regeneration run (first gas release) always has the slowest kinetics; these tendencies showed good reproducibility for all the composite material tested. The reason why we observed these different kinet ics is still under investigation in our lab, using *in situ* Raman exper iments. Work is also in progress to evaluate these reactive media for separating CO_2 from gas mixtures, in an attempt to see whether the separation selectivity toward CO_2 could be enhanced in the

same way as for the global capture capacity and reaction kinetics by using this type of composite material.

Acknowledgments

We would like to acknowledge the entire work group involved in the ORCHIDS project and the Carnot Institute ISIFoR (Institute for the Sustainable engIneering of Fossil Resources). We extend our thanks to the staff of the *Service Analyse et Procédés* of the University of Toulouse for their help. We also wish to thank Mathieu Molinier, Victor Cabrol and Sofiane Bekhti for their tech nical assistance and the Total E&P, "Gas Solutions" department for its financial backing. We would also like to thank Total for pro viding UMS 3360 DMEX with the Zeiss Xradia Versa 510 used to carry out the tomographic acquisitions reported in this article.

Appendix A. Supplementary data

Supplementary data associated with this article can be found, in the online version, at http://dx.doi.org/10.1016/j.cej.2017.05.038.

References

[1] H.M. Powell, The structure of molecular compounds. Part IV. Clathrate compounds, J. Chem. Soc. (1948) 61–73.
[2] J.L. Atwood, J.W. Steed, Encyclopedia of Supramolecular Chemistry, vol. 1, CRC Press, Taylor & Francis Group, Boca Raton, 2004.
[3] E.D. Sloan, Fundamental principles and applications of natural gas hydrates, Nature 426 (2003) 353–363.
[4] H. Dashti, L. Zhehao Yew, X. Lou, Recent advances in gas hydrate-based CO_2 capture, J. Nat. Gas Sci. Eng. 23 (2015) 195–207.
[5] P. Babu, P. Linga, R. Kumar, P. Englezos, A review of the hydrate based gas separation (HBGS) process for carbon dioxide pre-combustion capture, Energy 85 (2015) 261–279.
[6] J.-P. Torré, M. Ricaurte, C. Dicharry, D. Broseta, CO_2 Enclathration in the presence of water-soluble hydrate promoters: hydrate phase equilibria and kinetic studies in quiescent conditions, Chem. Eng. Sci. 82 (2012) 1–13.
[7] J.-P. Torré, D. Haillot, S. Rigal, R.W. de Souza Lima, C. Dicharry, J.-P. Bedecarrats, 1,3 dioxolane versus tetrahydrofuran as promoters for CO_2-hydrate formation: thermodynamics properties, and kinetics in presence of sodium dodecyl sulfate, Chem. Eng. Sci. 126 (2015) 688–697.
[8] Herri, J.-M., Kwaterski, M., Galfré, A., Brantuas, P., Cameirão, A., Ouabbas, Y., Bouillot, B., Sinquin, A., Broutin, P., Liebenthal, U., Kather, A., CO2 capture by using hydrates: From experimental evidences to economic impossibility as a post combustion process. Proc. of the 8th Int. Conf. on Gas Hydrates (2014) 28th July to 1st August 2014, BEIJING, China.
[9] M. Ricaurte, C. Dicharry, D. Broseta, X. Renaud, J.-P. Torré, CO_2 Removal from a CO_2–CH_4 gas mixture by clathrate hydrate formation using THF and SDS as water-soluble hydrate promoters, Ind. Eng. Chem. Res. 52 (2013) 899–910.
[10] M. Ricaurte, C. Dicharry, X. Renaud, J.-P. Torré, Combination of surfactants and organic compounds for boosting CO_2 separation from natural gas by clathrate hydrate formation, Fuel 122 (2014) 206–217.
[11] K.W. Han, Y.J. Lee, J.S. Jang, T.I. Jeon, J. Park, T. Kawamura, Y. Yamamoto, T. Sugahara, T. Vogt, J.-W. Lee, Y. Lee, J.-H. Yoon, Fast and reversible hydrogen storage in channel cages of hydroquinone clathrate, Chem. Phys. Lett. 546 (2012) 120–124.
[12] J.-W. Lee, P. Dotel, J. Park, J.-H. Yoon, Separation of CO_2 from flue gases using hydroquinone clathrate compounds, Korean J. Chem. Eng. 12 (2015) 2507–2511.
[13] T.A. Strobel, Y. Kim, G.S. Andrews, J.R. Ferrell III, C.A. Koh, A.M. Herring, E.D. Sloan, Chemical–clathrate hybrid hydrogen storage: storage in both guest and host, J. Am. Chem. Soc. 130 (2008) 14975–14977.
[14] J.-W. Lee, J.-H. Yoon, Preferential occupation of CO_2 molecules in hydroquinone clathrates formed from CO_2/N_2 gas mixtures, J. Phys. Chem. C 115 (2011) 22647–22651.
[15] Y.-J. Lee, K.W. Han, J.S. Jang, T.-I. Jeon, J. Park, T. Kawamura, Y. Yamamoto, T. Sugahara, T. Vogt, J.-W. Lee, Y. Lee, J.-H. Yoon, Selective CO_2 trapping in guest-free hydroquinone clathrate prepared by gas phase synthesis, Chem. Phys. Chem. 12 (2011) 1056–1059.
[16] Y.N. Kazankin, A.A. Palladiev, A.M. Trofimov, Study of heterogeneous equilibria for noble gas – HQ clathrate systems. Part I: phase diagrams, Zh. Obshch. Khim. 42 (1972) 2607–2611.
[17] Y.N. Kazankin, A.A. Palladiev, A.M. Trofimov, Study of heterogeneous equilibria for noble gas – HQ clathrate systems. Part II: clathration isotherms, Zh. Obshch. Khim. 42 (1972) 2611–2615.
[18] J.H. Van der Waals, J.C. Platteeuw, Thermodynamic properties of quinol clathrates, Recl. Trav. Chim. Pays-Bas 75 (1956) 912–918.
[19] Van der Waals, J.H., Platteeuw, J.C., Clathrate solutions. Adv. Chem. Phys., Vol. 2 (ed I. Prigogine), John Wiley & Sons Inc, 1959.
[20] R. Coupan, M. Chabod, C. Dicharry, J. Diaz, C. Miqueu, J.-P. Torré, Experimental determination of phase equilibria and occupancies for CO_2, CH_4, and N_2 hydroquinone clathrates, J. Chem. Eng. Data 61 (2016) 2565–2572.
[21] J.-P. Torré, R. Coupan, M. Chabod, E. Péré, S. Labat, A. Khoukh, R. Brown, J.-M. Sotiropoulos, H. Gornitzka, CO_2–Hydroquinone clathrate: synthesis, purification, characterization and crystal structure, Cryst. Growth Des. 16 (2016) 5330–5338.
[22] S.A. Allison, R.M. Barrer, Clathration by phenol and quinol. Part. II Kinetics, Trans. Far. Soc. 64 (1968) 557–565.
[23] S.P. Jiang, A review of wet impregnation – an alternative method for the fabrication of high performance and nano-structured electrodes of solid oxide fuel cells, Mater. Sci. Eng., A 418 (2006) 199–210.
[24] Hemati, M., Steinmetz, D., Chaudret, B., Philippot, K., Fabrication de catalyseur d'un nouveau type par imprégnation en lit fluidise, Patent EPI-PCT/FR 02/01795, 2001.
[25] L. Barthe, S. Desportes, M. Hemati, K. Philippot, B. Chaudret, Synthesis of supported catalysts by dry impregnation in fluidized bed, Chem. Eng. Res. Des. 85 (2007) 767–777.
[26] L. Barthe, M. Hemati, K. Philippot, B. Chaudret, Dry impregnation in fluidized bed: drying and calcination effect on nanoparticles dispersion and location in a porous support, Chem. Eng. Res. Des. 8 (2008) 349–358.
[27] L. Barthe, S. Desportes, D. Steinmetz, M. Hemati, Metallic salt deposition on porous particles by dry impregnation in fluidized bed: effect of drying conditions on metallic nanoparticles distribution, Chem. Eng. Res. Des. 87 (2009) 915–922.
[28] L. Barthe, M. Hemati, K. Philippot, B. Chaudret, A. Denicourt-nowicki, A. Roucoux, Rhodium colloidal suspension deposition on porous silica particles by dry impregnation: study of the influence of the reaction conditions on nanoparticles location and dispersion and catalytic reactivity, Chem. Eng. J. 151 (2009) 372–379.
[29] S. Desportes, D. Steinmetz, M. Hemati, K. Philippot, B. Chaudret, Production of supported asymmetric catalysis in a fluidized bed, Powder Technol. 157 (2005) 12–19.
[30] G. Peyronel, G. Barbieri, On some new clathrates of hydroquinone, J. Inorg. Nucl. Chem. 582–585 (1958).
[31] X. Li, Q. Yin, W. Chen, J. Wang, Solubility of hydroquinone in different solvents from 276.65 to 345.10 K, J. Chem. Eng. Data 51 (2006) 127–129.
[32] J.-W. Fulton, Selecting the catalyst configuration, Chem. Eng. 93 (1986) 97–101.
[33] A. Lekhal, B. Glasser, J.G. Khinast, Impact of drying on catalyst profile of supported impregnation catalysts, Chem. Eng. Sci. 56 (2001) 4473–4487.
[34] M. Hemati, R. Cherif, K. Saleh, V. Pont, Fluidized bed coating and granulation: influence of process-related variables and physicochemical properties on the growth kinetics, Powder Technol. 130 (2003) 18–34.
[35] F. Khaddour, A. Knorst-Fouran, F. Plantier, M.M. Piñeiro, B. Mendiboure, C. Miqueu, A fully consistent experimental and molecular simulation study of methane adsorption on activated carbon, Adsorption 20 (2014) 649–656.
[36] R.W. Coutant, Solventless preparation of hydroquinone clathrates, J. Org. Chem. 39 (1974) 1593–1594.
[37] H.G. McAdie, Thermal decomposition of molecular complexes: II. β-quinol clathrates, Can. J. Chem. 41 (1963) 2137–2143.
[38] H.G. McAdie, Thermal decomposition of molecular complexes: IV. Further studies of the β-quinol clathrates, Can. J. Chem. 44 (1966) 1373–1386.
[39] M. Thommes, K. Kaneko, A.V. Neimark, J.P. Olivier, F. Rodriguez-Reinoso, J. Rouquerol, K.S.W. Sing, Physisorption of gases, with special reference to the evaluation of surface area and pore size distribution (IUPAC Technical Report), Pure Appl. Chem. 87 (2015) 1051–1069.
[40] Chiekh, N.S.-B., Evaporation en milieu poreux en présence de sel dissous. PhD Thesis INP Toulouse, France, 2006.
[41] V.R. Belosludov, Y.A. Dyadin, G.N. Chekhova, B. Kolesov, S.I. Fadeev, Hydroquinone clathrates and the theory of clathrate formation, J. Inclusion Phenom. 3 (1985) 243–260.
[42] M.M. Conde, J.-P. Torré, C. Miqueu, Revisiting the thermodynamic modelling of type I gas-hydroquinone clathrates, Phys. Chem. Chem. Phys. 18 (2016) 10018–10027.
[43] J.N. Helle, D. Kok, J.C. Platteeuw, J.H. Van der Waals, Thermodynamic properties of quinol clathrates III, Recl. Trav. Chim. Pays-Bas 81 (1962) 1068–1074.
[44] J.W. Steed, D.R. Turner, K.J. Wallace, Core Concepts in Supramolecular Chemistry and Nanochemistry, John Wiley & Sons, Chichester, England, 2007.
[45] D.E. Palin, H.M. Powell, The structure of molecular compounds. Part VI. The β-type clathrate compounds of quinol, J. Chem. Soc. (1948) 815–821.

Creating innovative composite materials to enhance the kinetics of CO_2 capture by hydroquinone clathrates

Romuald COUPAN [1], Frédéric PLANTIER [2], Jean-Philippe TORRÉ [1,], Christophe DICHARRY [1], Pascale SÉNÉCHAL[3], Fabrice GUERTON [3], Peter MOONEN [1,3], Abdel KHOUKH [4], Sid Ahmed KESSAS [5], Mehrdji HEMATI [5]*

AUTHOR AFFILIATIONS:

1. CNRS/TOTAL/UNIV PAU & PAYS ADOUR, Laboratoire des Fluides complexes et leurs Réservoirs-IPRA, UMR5150, 64000, PAU, France

2. CNRS/TOTAL/UNIV PAU & PAYS ADOUR, Laboratoire des Fluides complexes et leurs Réservoirs-IPRA, UMR5150, 64600, ANGLET, France

3. UNIV PAU & PAYS ADOUR, CNRS, DMEX-IPRA, UMS 3360, 64000, Pau, France

4. UNIV PAU & PAYS ADOUR, CNRS – UMR 5254 – *Institut des Sciences Analytiques et de Physico-Chimie pour l'Environnement et les Matériaux* (IPREM), Hélioparc, Avenue du Président Pierre Angot, Pau F-64000, France.

5. Université de Toulouse – Paul Sabatier, CNRS – UMR 5503 – *Laboratoire de Génie Chimique* (LGC), ENSIACET, INPT, 5 rue Paulin Talabot, BP 1301, Toulouse F-31106, France.

* CORRESPONDING AUTHOR: Jean-Philippe TORRE. Address: CNRS/TOTAL/UNIV PAU & PAYS ADOUR, Laboratoire des Fluides complexes et leurs Réservoirs-IPRA, UMR5150, 64000, PAU, France. Tel. +335 40 17 51 09. Email: jean-philippe.torre@univ-pau.fr

SUPPLEMENTARY MATERIAL

1. INFORMATION CONCERNING THE NATIVE SUPPORT MATERIALS

The native support materials − SiliaFlash® (SF) and SiliaSphere® (SS) silica particles − used in this study underwent particle size characterization and gas porosimetry in order to experimentally determine their textural parameters. Our experimental data and those provided by the supplier are given in Table SI1 and Table SI2 respectively. As the batch of SF particles presented a large size dispersion (i.e. from 200 to 1,000 µm), it had to be separated into two fractions to allow homogenous fluidization: a low fraction of particles from 200 to 500 µm (called L-SF below) and a high fraction of SF particles from 500 to 1,000 µm (referred to as H-SF below).

Note that the SS particles were not evaluated by gas porosimetry, as the PSD was out of the measurement range of the equipment. For the native SF particles, the PSD analysis revealed mesopores of about 38 ± 5 nm, in good agreement with supplier data (pore diameter of 33 nm provided).

Table SI1. Textural parameters of native SiliaFlash® (SF) and SiliaSphere® (SS).

Support material	***L-SF***	***H-SF***	***SS***
d_{10} ***(µm)***	127	478	183
d_{50} ***(µm)***	326	748	249
d_{90} ***(µm)***	587	804	341
Mean particle diameter (µm)	306	710	242
Mean pore diameter (nm)	38		-
Porous volume (cm^3/g)	0.89		-
Specific area (m^2/g)	144		-

Table SI2. Physical properties of native SiliaFlash® (SF) and SiliaSphere® (SS) given by the supplier.

Support material	*SF*	*SS*
Particle diameter (µm)	200 – 1,000	200 – 500
Mean pore diameter (nm)	33	99
Porous volume (cm^3/g)	1.28	0.83
Apparent density (g/cm^3)	0.583	0.790
Particle density (g/cm^3)	2.29	2.29
Porosity fraction	0.75	0.64
Specific area (m^2/g)	155	57
pH	4.3	7.4

The operating conditions applied for developing the composite materials by Dry Impregnation (DI), particularly the minimum fluidization velocities of the particles obtained at room temperature, are listed in Table SI3.

Table SI3. Operating conditions applied for the DI of SiliaFlash® (SF) and SiliaSphere® (SS).

Support material	*H-SF*	*L-SF*	*SS*
Fluidized bed temperature (K)	308	308	308
Initial mass of support material (g)	310	330	345
Minimal fluidization velocity (m/s)	0.110	0.021	0.017
Fluidization gas flow-rate (m^3/h)	7.80	7.80	7.38
Spraying gas flow-rate (Nm^3/h)	1.2	1.2	1.2
HQ mass fraction of solution	0.31	0.31	0.31
Mass of sprayed solution (g)	383	198	556
Theoretical precursor content ($g^{HQ}/g^{support}$)	0.38	0.19	0.50

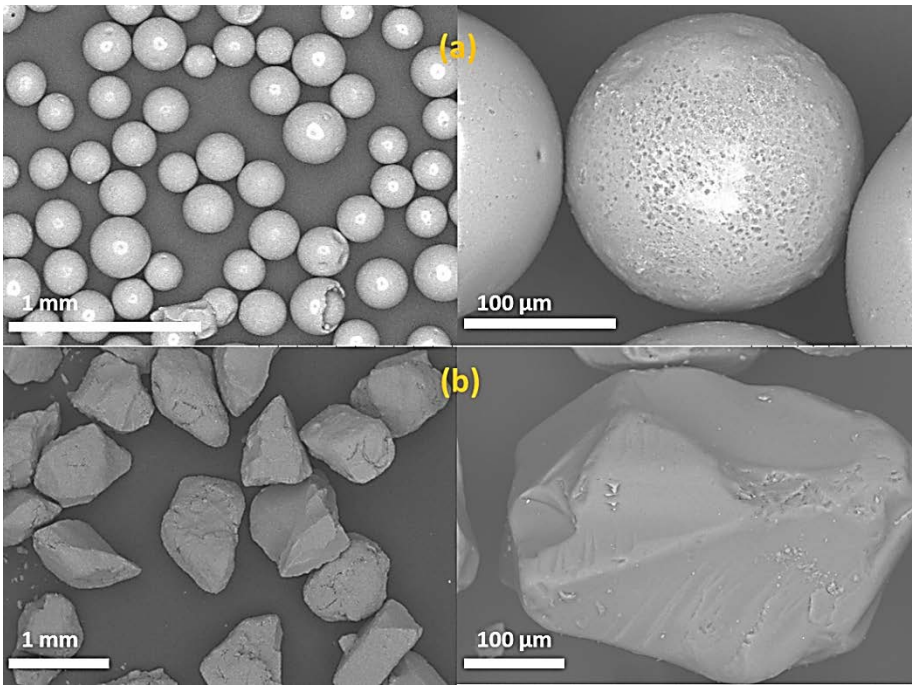

Figure SI1. SEM images of native silica particles: (a) SS particles; (b) H-SF particles. Images obtained with a tabletop microscope HITACHI TM3000 equipped with an EDS SwiftED3000 detector from Oxford Instruments.

2. TECHNICAL DETAILS OF ANALYTICAL TECHNIQUES

The mean particle diameter and particle size distribution were evaluated by sieving and by using a laser diffraction particle size analyzer from Malvern Instruments (model Mastersizer 2000). The laser diffraction particle size analyzer works for particles of about 0.02 µm to 2,000 µm.

The morphology of the particles was obtained using a field emission gun scanning electron microscope (SEM-FEG) from JEOL (model JSM 7100F TTLS). This SEM is equipped with an energy dispersive X-ray (EDX) spectrometer. The EDX technique detects X-rays emitted by the sample while it is being bombarded by an electron beam and is able to characterize the elemental composition of the surface analyzed.

The precursor content, defined as the mass of HQ per unit mass of support, was determined by thermogravimetric analysis (TGA) by measuring the mass loss rate of the sample subjected to a temperature ramp from ambient temperature to 773 K in an oxidizing atmosphere (air). The thermal signature of the impregnated compound was verified by differential scanning calorimetry (DSC). A Model Q600 analyzer from TA Instruments was used to perform both TGA and DSC.

The attrition resistance was determined by a simple attrition test. A sample of the composite material was sieved for 3 hours and its precursor content was measured by TGA. The value obtained was compared with the precursor content of the original sample.

The textural parameters – specific area, total pore volume, and pore size distribution (PSD) – were estimated from N_2 adsorption–desorption isotherms at 77 K using an automatic Micromeritics TriStar II 3020 system. This system can be used to evaluate mesoporous materials (i.e. materials with a pore size of 2 to 50 nm) with a specific area reaching several thousands of m^2/g. Before the measurements were taken, samples were purified at 308 K and 10 Pa for 24 hours. Specific areas were determined based on the Brunauer-Emmett-Teller (BET) method [Brunauer, S., Emmett, P.H., Teller, E., 1938. Adsorption of gases in multimolecular layers. J. Am. Chem. Soc. 60, 309-319]. Both the total pore volume and the pore size distribution were calculated using the Barrett-Joyner-Halenda (BJH) method [Barrett, E. P., Joyner, L.G., Halenda, P.P., 1951. The determination of pore volume and area distributions in porous substances. I. Computations from nitrogen isotherms. J. Am. Chem. Soc. 73, 373–380] applied to the desorption branch of the N_2 isotherm.

Structural data were obtained by cross-polarization / magic angle spinning (CP/MAS) solid-state ^{13}C NMR experiments using a Bruker Avance 400 spectrometer. The sample was placed in a zirconia rotor of 7 mm and the spectra were collected at ambient temperature at a resonance frequency of 100.61 MHz and a magic angle spinning rate of 7 kHz. The contact

time and pulse delay were 3.8 ms and 5 s respectively. Chemical shifts were referenced to tetramethylsilane at 0 ppm and carbonyl signal of glycine at 176 ppm as external reference.

The three-dimensional microstructure was obtained by X-ray tomography using a Zeiss Xradia Versa 510. Samples were subjected to the ambient test conditions (28°C) for at least 24h prior to each scan to ensure thermal equilibrium. For each scan, 2001 16 bit radiographs are acquired, while rotating the sample over 360°. The acquisition settings were selected based on the recommendations of the manufacturer of the tomograph [Zeiss, 2016. Zeiss Xradia Versa User's Guide]. 3D tomographic reconstruction was performed using the filtered back projection algorithm, as implemented in XMReconstructor [Zeiss, 2016. Zeiss Xradia Versa User's Guide], using a Gaussian filter with a unit kernel width. Data analysis and visualization was performed using Fiji [Schindelin J., Arganda-Carreras I., Frise E., Kaynig V., Longair M., Pietzsch T., Preibisch S., Rueden C., Saalfeld S., Schmid B., Tinevez J. Y., White D. J., Hartenstein V., Eliceiri K., Tomancak P., Cardona A., 2012. Fiji: an open-source platform for biological-image analysis. Nat Methods, 9, 676-682].